Modeling of Casting, Welding and Advanced Solidification Processes XII, Vancouver, Canada, June 7-14, 2009 *Edited by S. Cockroft et al.*
TMS (The Minerals, Metals & Materials Society), 2009

EXPLICIT COUPLED THERMO-MECHANICAL FINITE-ELEMENT MODEL OF CONTINUOUS CASTING OF STEEL IN FUNNEL MOLDS

Seid Koric[1], Lance C. Hibbeler[2], and Brian G. Thomas[2]

[1]National Center for Supercomputing Applications-NCSA
[2]Department of Mechanical Science and Engineering,
University of Illinois at Urbana-Champaign,
1206 West Green Street, Urbana, Illinois USA, 61801

Keywords: Continuous Casting, Solidification, Explicit, Finite Element, Thermal-stress models, numerical methods, ABAQUS, 3-D, Stress analysis, Parallel Computational Benchmarks

Abstract

A three-dimensional transient explicit finite-element method is applied to simulate the coupled and highly-nonlinear thermo-mechanical phenomena that occur during steel solidification in continuous casting of thin slabs in a funnel mold. Variable mass scaling is used to efficiently model the phenomena in their natural time scale using a Lagrangian formulation. The model features an efficient and robust local-global viscoplastic integration scheme to solve the elastic-viscoplastic constitutive equations of solidifying steel [1], using a VUMAT subroutine in ABAQUS/Explicit [2], which varies greatly with temperature, strain rate, steel phase, and composition. The model is applied to simulate temperature and stress development in typical repeating segment of the solidifying shell in a continuous casting funnel mold using realistic temperature-dependent properties and including the effects of ferrostatic pressure, narrow face taper, and mechanical contact, and thermal-mechanical coupling through the size of the interfacial gap. Explicit temperature and stress results as well as computational efficiency are compared with the results of an implicit formulation. The explicit formulation shows significant advantages for these large contact-solidification problems on parallel computers.

Introduction

Thermal-mechanical simulation is important to understand the formation of cracks, surface-shape problems, and other defects that affect commercial processes such as continuous casting of thin steel slabs in a funnel mold. The few seconds the steel spends in the mold are critical because most of the defects in the final product arise in the mold. Stresses and strains caused by thermal contraction, interaction with the mold walls, or other mechanical forces can generate cracks that can lead to catastrophic breakouts, or fill with segregated liquid and cause permanent defects in the final product.

However, the complexity of transient phenomena that govern this process presents a serious obstacle to accurate modeling. These phenomena include visco-plastic constitutive laws which depend on temperature, composition, and phase; a liquid/mushy zone that involves composition-dependent segregation, latent-heat evolution, and microstructural effects; temperature-dependent material properties; intermittent contact between the solidified shell and mold surfaces; and

coupling between the heat transfer and stress analysis through the changing thickness of the shell-mold interfacial gap.

Most previous thermal-mechanical models of continuous casting have applied finite-element methods with implicit solution methods [1,3-16]. This is due to their efficiency over finite-difference and finite-volume methods in fast, stable convergence of the highly-coupled and stiff nonlinearities typically encountered in stress problems, especially with complex geometries.

When fluid flow in the liquid pool must be coupled together with mechanical behavior in the solidifying shell, a few recent papers have adopted an Arbitrary Lagrangian Eulerian (ALE) formulation [11,12,13]. Despite the modeling advantages of a single simulation that combines fluid flow, solidification, and mechanical behavior, the practical application of ALE method is hampered by its complexity, its need for 3D remeshing procedures, and convergence problems. Furthermore, extra complexity is needed to account for the advection of material through the computational grid and to update the associated time-dependent variables. Risso et al. [12] found that an ALE axisymmetric model of a billet casting had a higher computational cost than a pure Lagrangian generalized plane strain model and recommended the latter for future work.

The vast majority of previous solidification models have adopted implicit finite-element analysis in a Lagrangian frame of reference, by tracking a slice through the strand as it moves down the caster, within a variety of one- and two-dimensional (1D and 2D) domains [1,3-10,14,15,26], and a recent analysis with a 3D domain [2,16]. Although Lagrangian elements sometimes experience distortion problems when the material is severely deformed, this is not an issue in the solid and mushy regions of castings. In solidification problems, cracks will form if the strains exceed only a few percent, so a small-strain theory can be accurately applied to investigate thermal-mechanical behavior up to the initiation of cracks. Cracks can be predicted with these models with the aid of damage criteria [15]. Furthermore, the advective terms and history-dependent variable(s) can be easily updated with Lagrangian elements. Care must be taken in liquid regions to allow volumetric flow while avoiding excessive strain.

Integration of time-dependent visco-plastic constitutive laws is a very challenging computational task due to their numerical stiffness. Koric and Thomas [1] implemented a robust local viscoplastic integration scheme from an in-house code CON2D [9,10,15,] into the commercial implicit finite element package ABAQUS/Standard via its user defined material subroutine UMAT, which has opened the door for realistic large-scale uncoupled 3D computational modeling of complex solidification processes [16]. However, coupled 3D problems with reasonable mesh resolution are difficult to solve, owing to memory and speed limitations, even on supercomputers. Lately, a cost-effective explicit time-integration solution method on the global level from the explicit finite-element package ABAQUS/Explicit is linked with the above efficient and robust local viscoplastic integration scheme via a VUMAT subroutine [2] enabling an effective and efficient tool to realistically model coupled thermo-mechanical behavior in large solidification problems involving complex interacting phenomena. Both models are verified with a semi-analytical solution [17], and then applied to simulate 2D and 3D transverse sections of various slab casters under realistic operating conditions as they move down the mold [16,25,26] including comparisons with plant measurements [25,26].

Model Description

The transient heat conduction equation and the mechanical equilibrium equations are solved in both 2-D and 3-D domains of molten steel solidifying in a thin-slab casting funnel mold.

Explicit formation for both time and spatial integration is compared with a conventional implicit formulation, described in detail in previous work [1].

Heat Transfer Model

The explicit model used here solves the standard heat conduction equation using the finite-element method for spatial integration and marches through time using the fully explicit "forward finite-difference" method:

$$\{T\}^{t+\Delta t} = \{T\}^{t} + \{\dot{T}\}^{t}\Delta t \tag{1}$$

A lumped thermal capacitance matrix, based on temperatures at the previous time step, is inverted analytically, which enables an explicit solution of the finite element equations. The time step size is limited by the standard stability criterion for the forward-difference operator:

$$\Delta t \leq \min\left(\frac{\rho c_p L_e^2}{2k}\right) \tag{2}$$

where L_e is the characteristic length of the smallest element in the domain, k is thermal conductivity, ρ is density, and specific heat c_p is found from the slope of the enthalpy-temperature curve, which includes the latent heat of solidification linearly distributed between the liquidus and solidus temperatures [18].

Stress Model

The thermal strains from the temperature solution, the ferrostatic pressure, and contact with thermally-distorted mold walls, are all computed in this work and applied as thermal loads to an explicit stress model. Stress in the solidifying steel shell is calculated assuming an elastic-viscoplastic constitutive model, which involves highly nonlinear equations to relate strain rate with stress, temperature, and inelastic strain. Separate equations are used for austenite and delta-ferrite, which are explained in previous work [15].

The explicit finite element method used here differs notably from previous methods in that an inertial term is added to the mechanical governing equation for mechanical equilibrium:

$$\nabla \cdot \boldsymbol{\sigma} = \rho \mathbf{g} + \rho \ddot{\mathbf{u}} \tag{3}$$

where $\boldsymbol{\sigma}$ is the Cauchy stress tensor, $\rho\mathbf{g}$ is the body force vector due to gravity, and $\ddot{\mathbf{u}}$ is the acceleration vector. The mechanical problem is formulated in terms of nodal accelerations and explicitly advances the kinematic state of the system from the previous time step without iteration. At the beginning of a time step, dynamic equilibrium is solved:

$$\left\{\ddot{u}^{t}\right\} = [M]^{-1}\left(\{P\}^{t} - \{S\}^{t}\right) \tag{4}$$

where $[M]$ is the diagonal "lumped" nodal mass matrix which is trivial to invert, and $\left\{\ddot{u}^{t}\right\}$ are the nodal accelerations at the beginning of the increment, The accelerations are integrated explicitly through time using the central-difference method, which calculates the change in velocity assuming constant acceleration over a small time step. This velocity change is added to

the velocity from the middle of the previous step to calculate the velocities at the middle of the current step:

$$\left\{\dot{u}^{t+\frac{\Delta t}{2}}\right\}=\left\{\dot{u}^{t-\frac{\Delta t}{2}}\right\}+\frac{\left(\Delta t^{t+\Delta t}+\Delta t^{t}\right)}{2}\left\{\ddot{u}^{t}\right\} \tag{5}$$

The velocities are integrated once more to calculate the displacement increment, which is then used to update the displacements at the end of the time step:

$$\left\{u^{t+\Delta t}\right\}=\left\{u^{t}\right\}+\Delta t^{t+\Delta t}\left\{\dot{u}^{t+\frac{\Delta t}{2}}\right\} \tag{6}$$

A numerical stability requirement limits the maximum time step size in the explicit method. In general, the critical time step is $\Delta t \le 2/\omega_{\max}$, where $\omega_{\max}$ is the highest frequency (largest eigenvalue) of the system. To avoid extracting eigenvalues, a more practical estimate of the stability limit is made using the dilatational wave speed c_d and the characteristic length L_e of the smallest element in the domain:

$$\Delta t \le \min\left(\frac{L_e}{c_d}\right) \qquad \text{where: } c_d=\sqrt{\frac{\lambda+2\mu}{\rho}} \tag{7}$$

where λ is the first Lamé constant, μ is the shear modulus, and ρ is the density of the element, which is chosen automatically to satisfy the user-defined critical time step. As the material density increases, the stability limit increases too, which lowers the computational cost. Density increase with so called mass scaling [22] is applied throughout this work insuring that changes in the mass and consequent increases in the inertial forces do not alter the quasi-static solution, by keeping the ratio of the kinetic energy to the total strain energy less than 5% [2].

Despite the large number of time steps needed for the explicit method, it is often more efficient than the implicit method, particularly when many expensive NR iterations are needed. Also, contact conditions are solved more easily using this explicit method [19,20]. Furthermore, complete coupling between the temperature and displacement fields is obtained automatically, given that the explicit method does not require iteration at the global level.

After solving for the displacements, and corresponding total strains at each time step, the constitutive equations are integrated at every material point to update the stress, using a user subroutine VUMAT in ABAQUS. Next, heat transfer coefficients are updated and internal thermal and mechanical forces are computed, and the solution proceeds to the next time step. Details of the coupled solution strategies in explicit and implicit models are given in [2].

Funnel Mold Continuous Casting Simulations

The mold region of the “CSP” thin slab casting process is shown in Figure 1. To enable a thinner mold than conventional slab casting, the funnel shape design provides the space needed for the submerged entry nozzle (SEN), which protects the molten steel from atmospheric contamination. This particular funnel design has flat, parallel sections in the center of the mold and near the narrow faces. The funnel gradually tapers down the mold, ending sharply into a rectangular cross-section at 850mm down the mold, which gives the slab its near-final shape.

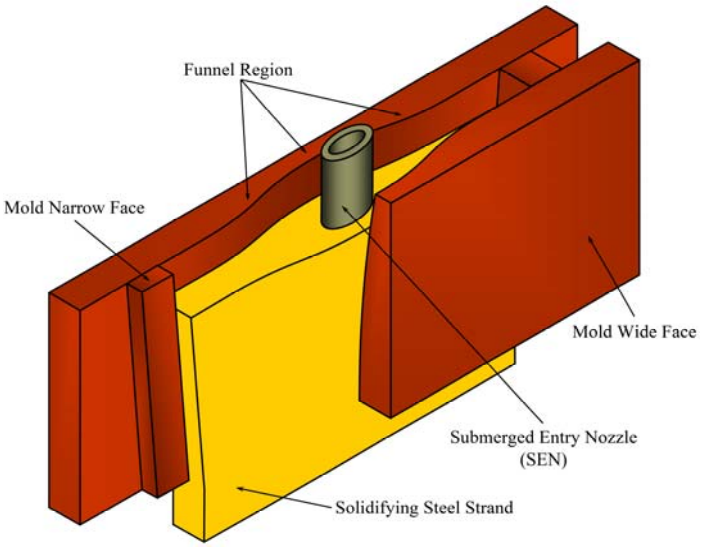

Figure 1: Schematic of thin slab casting

The dimensions of the funnel mold are shown in Figure 2, which also highlights the computational domain that takes advantage of quarter symmetry. Both the 2D and 3D models are applied to simulate a typical casting speed of 5.5 m/min. Attention is focused on the temperature and stress profiles at 5s, which corresponds to 460 mm down the 1100-mm mold length.

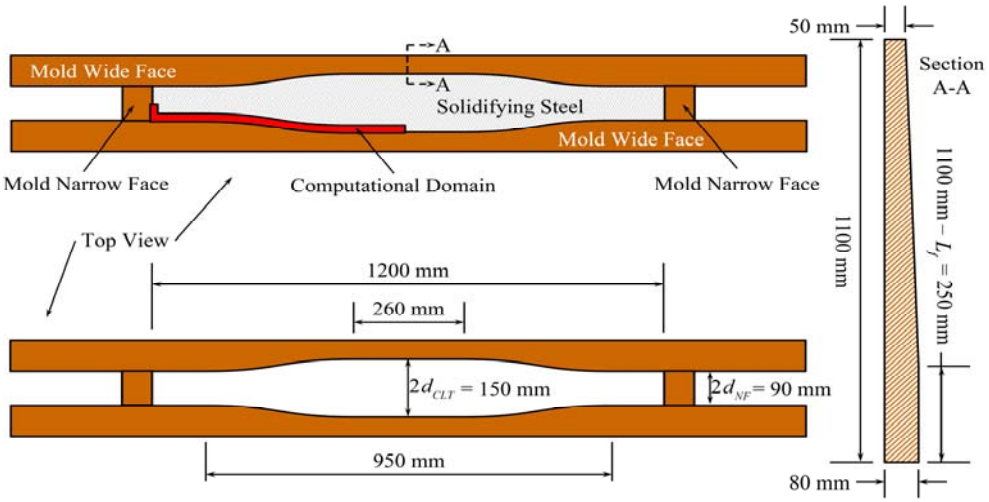

Figure 2. Funnel Mold Dimensions

Boundary and Initial Conditions

Continuous casting molds are given a taper to attempt to compensate for the shell shrinkage and ensure good contact (and thus uniform heat transfer) between the shell and the mold. The mold taper and changes in mold shape are included in this numerical model by prescribing the velocities of the mold contact surfaces as a function of time, consistent with distance down the mold according to the Lagrangian formulation The velocities were prescribed instead of displacements because defining the nodal displacements in the explicit model caused unrealistic behavior from acceleration spikes.

Mechanical contact between the steel shell surfaces and mold surfaces was imposed with a tangential friction factor of 0.1 [21]. The explicit method readily employed the standard ”hard” contact algorithm (penalty-based method) in ABAQUS [22] which is more robust than the contact algorithm in implicit code [2] Two-way coupling is necessary to capture the effects of

the evolving interfacial gap, given that the stress solution depends on the temperature field through thermal strain, and gap heat transfer depends on the gap distance calculated from the mechanical solution.

The heat conducted across the contacting surfaces is a strong function of the distance between the surfaces. The gap between the surfaces is computed in the stress analysis and used in the heat transfer analysis to define conduction across the interface. The gap heat transfer coefficient h_g is found according to:

$$h_g = h_o \qquad d \le d_0$$

$$h_g = \frac{1}{\frac{d}{k_{air}} + R_c} + h_{rad} \qquad d_0 < d \tag{8}$$

where d is the gap size, d_0 is the critical gap size (taken to be 0.1 mm in this work), k_{air} is the thermal conductivity of the gas in the gap, R_c is the contact resistance of the interface, h_{rad} is the effective heat transfer coefficient due to radiation, and h_0 is the gap heat transfer coefficient corresponding to a gap of size d_0. Values of these terms, which vary with temperature, and further details of this gap heat transfer calculation are given elsewhere [23,24]. Truncating the gap heat transfer coefficient at h_0 also facilitates comparison of the different models, forcing the coefficient to be constant for small gaps (less than d_0) in order to avoid changes in heat transfer due to minor changes in contact convergence.

The liquid steel inside the solidified shell exerts a pressure on the inside surface of the shell, known as the ferrostatic pressure (analogous to hydrostatic pressure), that increases linearly with distance below the liquid steel meniscus. This effect is included in the model as a distributed load applied outward at the surface of the steel shell [2]. The initial temperature of the simulated steel is uniformly 1540 ºC, equal to the temperature at which it is poured into the mold. The mold is maintained at a constant 150 ºC throughout the analysis, which is the approximate average value of the surface temperature in the mold.

Two-Dimensional Model

To simplify the numerical modeling of the continuous casting process, a transient Lagrangian domain is adopted, where the analysis follows a slice of material as it moves down through the casting machine at the casting speed. Relative to a "laboratory" frame of reference however, the process reaches steady state after a transient period following the start-up process or a change in casting conditions. For steel, this process has a high Péclet number (typically on the order of $2 \cdot 10^5$), meaning that advection heat transfer dominates over conduction in the axial (casting) direction. Thus, axial conduction can be neglected, and the 2D transient domain can reproduce the complete 3D steady temperature results. For the mechanical analysis, the most appropriate 2D approximation is a generalized plane strain condition, which requires that the axial strain components are all equal to the same constant value (since all model domains in this work take advantage of at least two-fold symmetry). The 2D analysis domain for the funnel mold consists of a thin L-shaped slice that is 17-mm thick in the transverse plane, as shown in Figure 3.

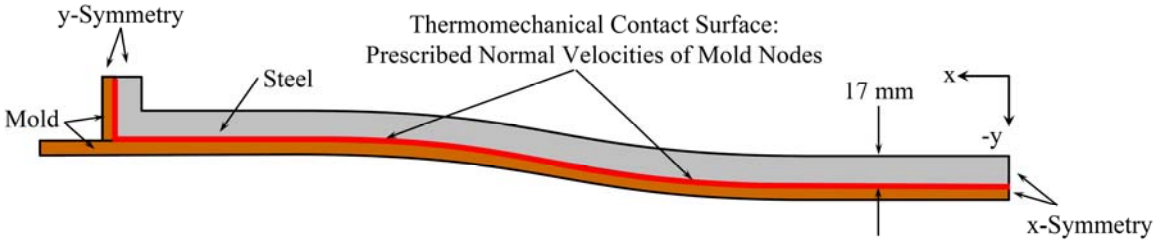

Figure 3. Two-Dimensional Funnel Model Boundary Conditions

This enables simulations of solidification up to almost twice the expected shell thickness at mold exit. To fairly compare the implicit and explicit analyses, both models used meshes consisting of a single layer of hexahedron elements, 2 mm thick in the casting direction. The generalized plane strain condition was imposed with constraint equations because ABAQUS/Explicit currently does not have generalized plane strain elements. The shell domain initially corresponds to the shape of the funnel mold at the meniscus. The deformation of the shell caused by moving down through the funnel shape was imposed by prescribing the y-velocities of the mold contact surfaces to appropriate functions of time and space.

A mesh of 29,169 elements (about 160,000 degrees of freedom) was chosen to capture the solidification phenomena for this problem. Contact stabilization in the form of viscous damping in the normal direction had to be applied to enable the implicit solver to complete a simulation. The explicit simulation required time steps of $5 \cdot 10^{-6}$ seconds to avoid divergence problems.

The explicit and implicit simulation results at 5 seconds (460 mm below the meniscus) are compared in Figures 4-7 for the same coarse mesh of 29,169 elements. In addition, a more refined mesh of 109,224 elements (about 543,000 degrees of freedom) was investigated for the explicit model to try to attenuate some of the numerical fluctuations.

Figures 4 and 5 show through-thickness profiles of temperature and tangential stress at the mold centerline.

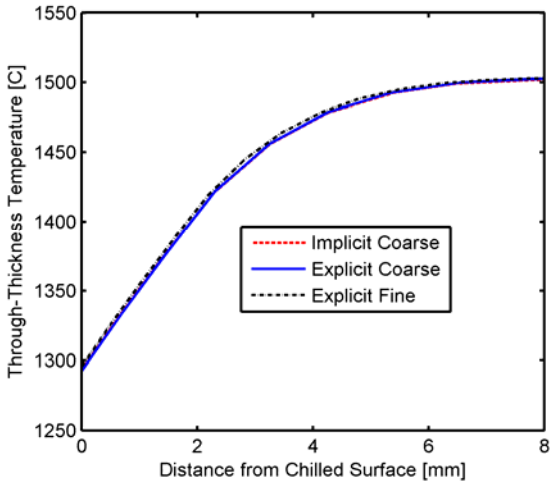

Figure 4. Through-Thickness Temperature Profiles

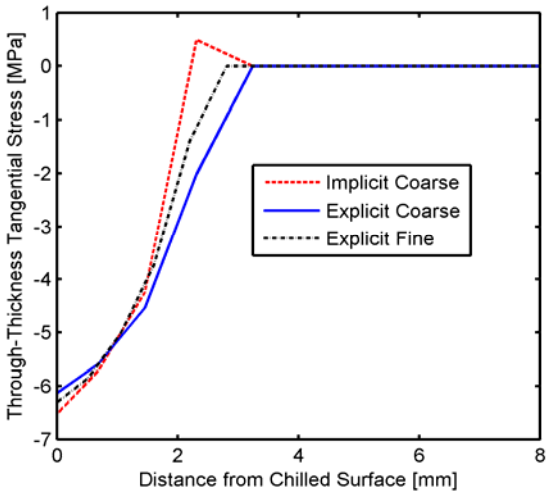

Figure 5. Through-Thickness Tangential Stress Profiles

Tangential stress (perpendicular to the dendrite growth direction) was computed during post-processing from the 2D stress transformation equation applied to the in-plane stress components. The angle of rotation is readily determined through the geometry of the mold. The explicit and implicit solutions match temperature results within 0.5 ºC for identical meshes. The refined

mesh with the explicit solver produces a smoother temperature profile. The explicit solutions predict less compressive stress on the surface than the implicit solution, and are also unable to capture the subsurface tensile stress peak that the implicit solution predicts. The more refined explicit solution matches closer to the implicit solution.

Figure 6 shows the surface temperature distribution on the wide face at 5 seconds below meniscus. The course-mesh explicit and implicit results generally match within about 0.5 ºC, and the refined mesh is about 2 ºC hotter. The funnel has a very slight 2D effect on the heat transfer, causing a small (about 1 ºC) decrease and increase from 130 mm to 302.5 mm and 302.5 to 475 mm, respectively, from the centerline.

A small spike in the profiles around 475 mm from the centerline is caused by a small gap opening from a combination of the shell shrinking and the changing funnel shape pushing on the shell. This temperature difference augments the corresponding spike in the surface tangential stress as seen in Figure 7. The spike is more severe with the explicit model, owing to the large wave speed gradients.

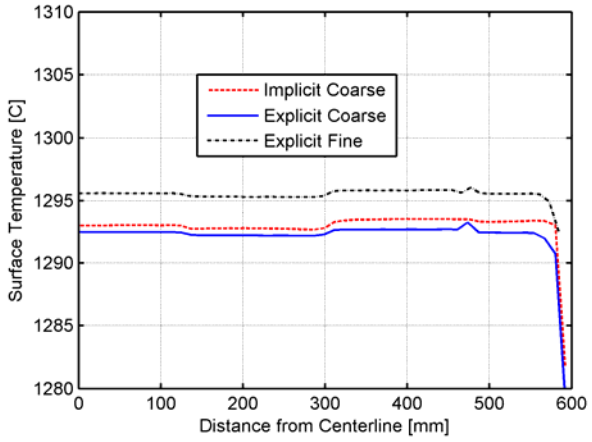

Figure 6. Wide Face Surface Temperature

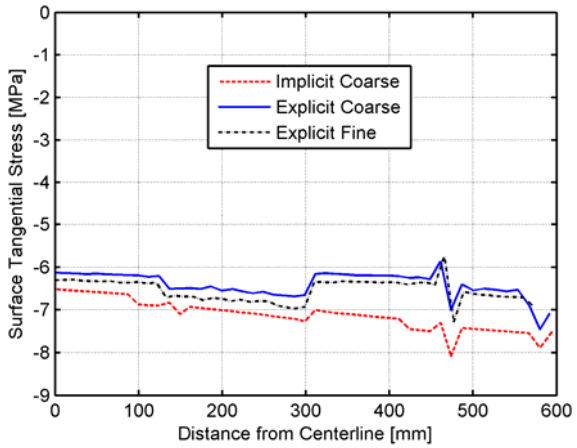

Figure 7. Wide Face Surface Tangential Stress

The funnel pushes the shell to "unbend" it, which alters the stress in the funnel region [26]. Although the bending stresses are most severe at the shell surface, the shell experiences compression through its entire thickness, which is partly due to squeezing by the narrow face of the mold. The implicit solution grows more compressive in the outer half of the mold. The differences between the implicit and explicit stress solutions are likely due to the different effects of mesh resolution on the different formulations, as well as the different contact algorithms used.

Three-Dimensional Model

A 3D explicit Lagrangian simulation was performed for a portion of the shell as it moves through the funnel mold. This model geometry is an extrusion of the 2D domain for a length of 100 mm in the casting direction, and each point in the material has its own "local time" based on when the point passes the meniscus. The changing shape of the mold face encountered by the moving shell is included in the model by means of a time- and spatially-dependent displacement function, which is expressed as normal velocity constraints on surface nodes, as described in detail elsewhere [2]. Figure 8 shows the boundary conditions on the analysis domain in the Lagrangian frame of reference.

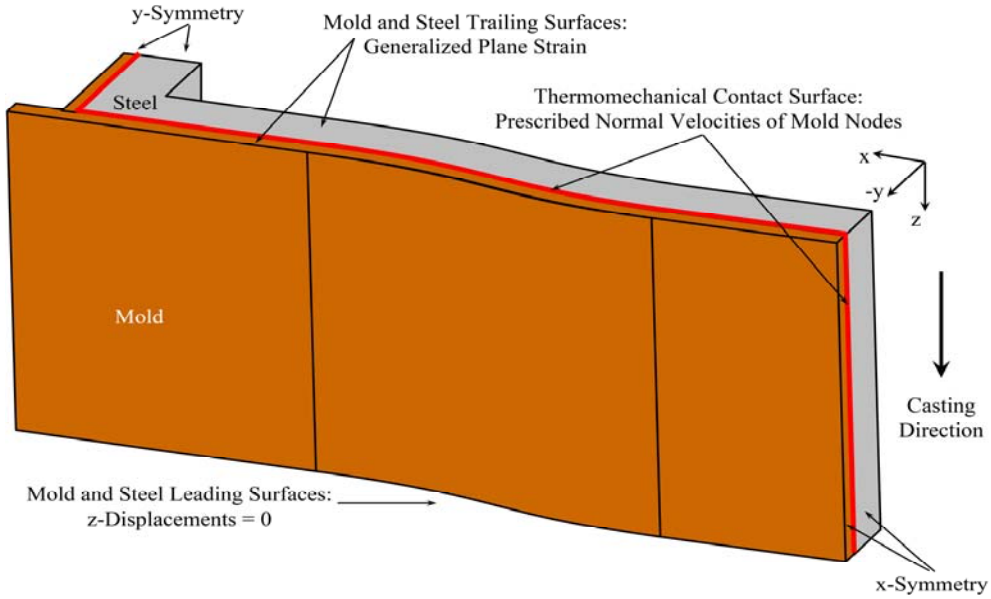

Figure 8. Three-Dimensional Funnel Model Boundary Conditions

Typical 3D results from the explicit model are shown in Figure 9. Surface temperatures are relatively uniform, except very near the corner, where 2D cooling exists. This is because the shell stays in reasonably close contact with the surface, so the gaps are all within the tolerance of 0.1 mm, which causes no change in heat conduction. The axial stress (in the casting direction) is one of the primary reasons for applying a 3D model. The relatively uniform stress distribution in the central region indicates that the funnel does not cause significant axial bending in top portions of this mold. Figure 9 clearly shows the complicated 3D state of stress that exists in the corner and off-corner regions, which the 2D models cannot capture correctly. This region is prone to transverse surface cracks in practice, caused by the axial stress.

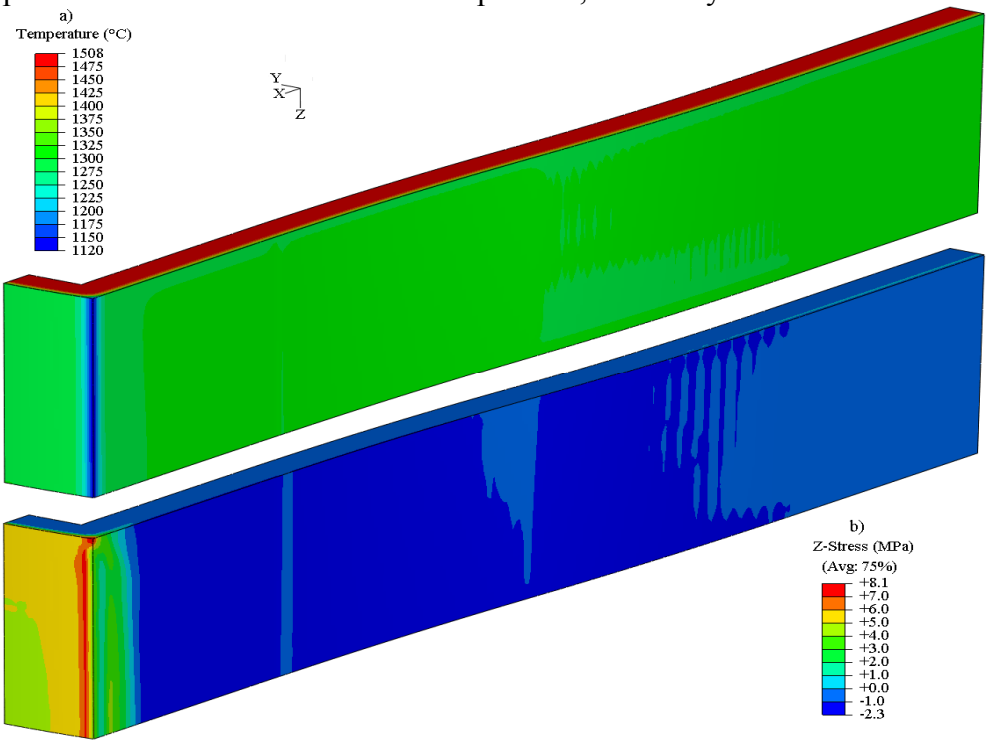

Figure 9. Three-dimensional surface contours at 5 seconds of a) temperature and b) z-stress (casting direction) predicted by the explicit model

The 2D and 3D model predictions are compared in Figures 10-13. Near the leading (bottom) and trailing (top) ends of the 3D model domain, "end effects" significantly alter the stress results. This is due to the lack of constraint, and extends about 15-mm. To make a realistic comparison, data was extracted from the 3D model in a plane 19 mm above the leading edge at 5 seconds into the simulation (relative to the leading edge). The corresponding 2D results are taken at 4.8 seconds into the simulation. The models match favorably, as seen in Figures 10-13.

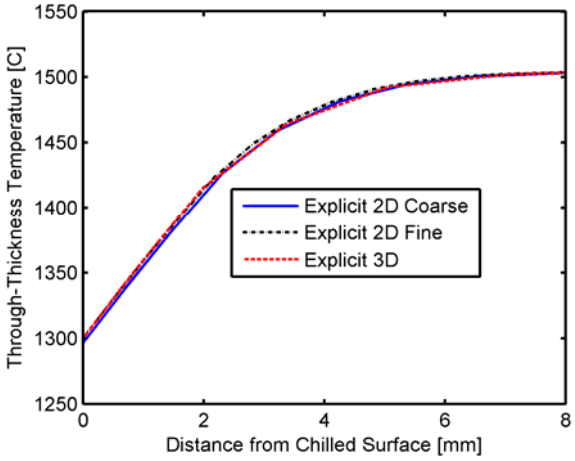

Figure 10. Through-Thickness Temperature Profiles

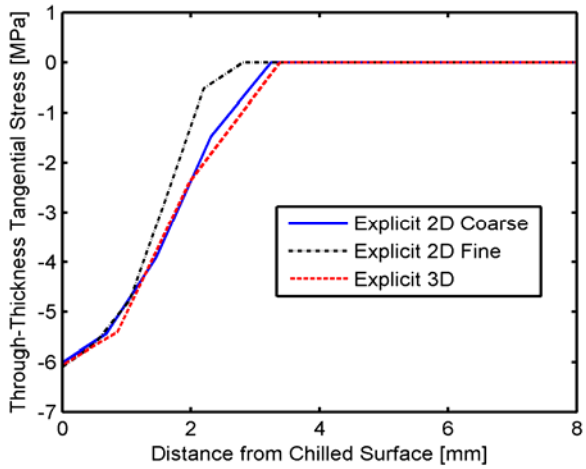

Figure 11. Tangential Stress Profiles through the shell thickness

The temperature profiles through the thickness (Figure 10) and along the perimeter (Figure 12) both match within about 3 ºC. This agreement validates the arguments made by many previous modelers that axial conduction is negligible with the large Péclet number of this continuous casting process. The 3D model stress results also match reasonably with the 2D predictions of tangential stress (generally within 0.5 MPa) both through the thickness (Figure 11) and along the perimeter (Figure 13). The 3D mesh refinement is the coarsest, which explains the slight variations between the three solutions. The agreement between these models validates the use of the generalized plane strain condition in 2D modeling of mechanical behavior of the shell in the mold, in the absence of axial bending.

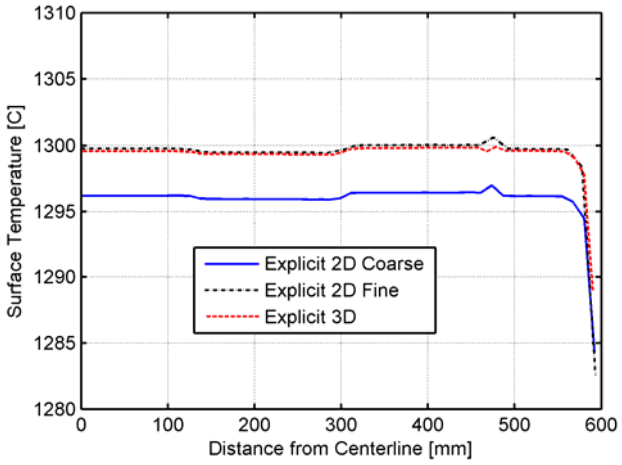

Figure 12. Comparison of model dimensions and mesh refinement on surface temperature

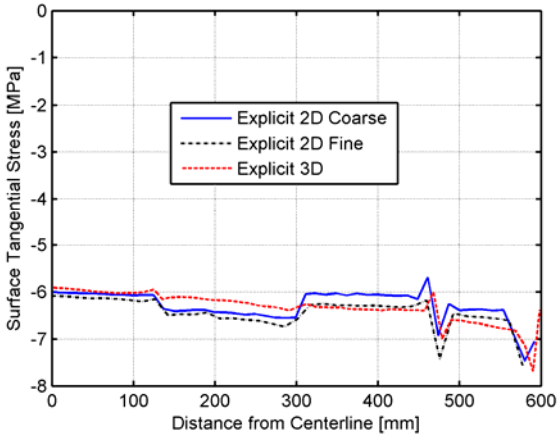

Figure 13. Comparison of model dimensions and mesh refinement on surface tangential stress predictions along shell perimeter

The results show a roughly parabolic increase in shell thickness down the mold, with corresponding decrease in surface temperature, and an almost linear temperature profile through

the shell, (Figure 10) which matches previous work. Surface stress is always in compression, while the subsurface is generally in slight tension. The new finding of this work is the effect of the funnel, which causes slight changes in temperature around the perimeter, owing to converging and diverging heat flow into the curved regions of the funnel mold (Figure 12). More importantly, the funnel causes additional bending stresses in the transverse plane (Figure 13). Unbending of the shell by the funnel 125-250mm from the centerline increases compression at the surface, with corresponding higher subsurface tension. Shell bending near the funnel edges (250-375mm) causes surface compression to decrease, while the subsurface tension is removed completely (Figure 11). Finally, the 3-D model predicts additional axial stresses, due to bending in the axial plane at the end of the funnel, where the mold walls become parallel. In addition, the shell lifts off of the mold in this region, creating a gap. These effects cannot be predicted with the 2-D model. These results have important implications for understanding cracks and other problems that affect the process.

Computational Performance

The performance of the explicit and implicit methods for the 2D funnel mold problem was evaluated for different mesh refinements and different numbers of parallel processor cores [2]. The two methods have similar efficiency for problems smaller than about 100,000 degrees of freedom (DOF). CPU time increases with DOF raised to the power of 1.41 for the explicit model, compared with 1.92 for the less-efficient implicit model. Thus, the explicit solver increasingly out-performs the implicit solver as problem size increases. In addition, the explicit solver needed only 5-10% of the implicit solver memory usage.

Conclusions

An explicit finite-element model of steel solidification has been developed and applied to simulate temperature and stress development in the solidifying steel shell of a funnel-mold continuous-casting.

Comparing 2-D and 3-D results shows that the assumptions of neglecting axial conduction and generalized plane strain (in the absence of axial bending) are reasonable when modeling continuous casting of steel.

The explicit model is more robust, requires less memory, and runs faster than the implicit model for problems with more than 100,000 degrees of freedom in either two or three dimensions. Furthermore, the explicit solver also scales better on parallel computers. This new model will be very beneficial in future analysis of large 3D, fully-coupled problems, especially on parallel computers with multi-core clusters.

Acknowledgements

The authors would like to thank the National Center for Supercomputing Applications at the University of Illinois at Urbana-Champaign (UIUC) for computational resources, the Continuous Casting Consortium at UIUC, the National Science Foundation (Grant CMMI-07-27620), and Corus Steel in IJmuiden, The Netherlands.

References

1. Koric S and Thomas BG. Efficient Thermo-Mechanical Model for Solidification Processes. *International Journal for Num. Methods in Eng* 2006; 66:1955-1989.

2. Koric S, Hibbeler LC, and Thomas BG. Explicit coupled thermo-mechanical model of steel solidification *International Journal for Num. Methods in Eng* 2008, published online DOI 10.1002/nme.2476.
3. Grill A, Brimacombe JK, and Weinberg F. Mathematical analysis of stress in continuous casting of steel. *Ironmaking Steelmaking* 1976; 3:38-47.
4. Kelly JE, Michalek KP, O'Connor TG. Thomas BG, and Dantzig JA. Initial development of thermal and stress fields in continuously cast steel billets. Metall. Trans. A 1988; 19A(10):2589-3602.
5. Kristiansson JO. Thermomechanical behavior of the solidifying shell within continuous casting billet molds-a numerical approach. *Journal of Thermal Stresses* 1984; 7:209-226.
6. Williams JR, Lewis RW, Morgan K. An elastic-viscoplastic thermal stress model with applications to the continuous casting of metals. *International Journal for Numerical Methods in Engineering* 1979; 14:1-9.
7. Boehmer JR, Funk G, Jordan M and Fett FN. Strategies for coupled analysis of thermal strain history during continuous solidification processes. *Advances in Engineering Software*, 1998; 29(7-9):679-697.
8. Farup I, Mo A. Two-phase modeling of mushy zone parameters associated with hot tearing. *Metall. Mater. Trans* 2000;31:1461-1472.
9. Zhu H. Coupled thermal-mechanical finite-element model with application to initial solidification. *Ph.D. Thesis*, University of Illinois 1993.
10. Chunsheng L and Thomas BG. Thermo-Mechanical Finite-Element Model of Shell Behavior in Continuous Casting of Steel. *Metal and Material Trans. B* 2005;35B(6):1151-1172.
11. Belet M, Fachinotti VD. ALE Method for solidification modeling. *Comput. Methods in Appl. Mech. and Engr.* 2004; 193:4355-4381.
12. Risso JM, Huespe AE, and Cardona A. Thermal stress evaluation in the steel continuous casting process. *International Journal for Numerical Methods in Engineering* 2006; 65(9):1355-1377.
13. Lewis RW, Postek EW, Han Z, and Gethin DT. A finite element model of squeeze casting process. *International Journal of Numerical Methods for Heat & Fluid Flow* 2006; 16(5):539-572.
14. Pascon F, Habraken AM. Finite element study of the effect of some local defects on the risk of transverse cracking in continuous casting of steel slabs. *Comput. Methods Appl. Mech. Engrg* 2007;196:2285-2299.
15. Li C, Thomas BG. Maximum casting speed for continuous cast steel billets based on sub-mold bulging computation. *85th Steelmaking Confernce Proceedings ISS-AIME, Nashville TN, 2002:109-130.*
16. Koric S, Thomas BG. Thermo-mechanical model of solidification processes with ABAQUS. *ABAQUS Users Conference (2007)*, Paris, France, 2007: 320-336.
17. J.H. Weiner and B.A. Boley, 1963 "Elastic-plastic thermal stresses in a solidifying body", J. Mech. Phys. Solids **11** 145-154.
18. Lewis RW, Morgan K, Thomas HR and Seetharamu KN. *The Finite Element Method in Heat Transfer Analysis*. Wiley: New York 1996.
19. Rebelo N, Nagtegaal JC, Taylor LM. Comparison of implicit and explicit finite element methods in the simulation of metal forming processes. *In Chenot, Wood, Zienkiewicz (Eds.), Numerical Methods in Industrial Forming Processes* 1992; 99–108.
20. Harewood FJ, McHugh PE. Comparison of implicit and explicit finite element methods using crystal plasticity. *Comp. Mat. Science* 2007; 39:481-494.
21. Meng Y, Thomas BG, Polycarpou AA, Prasad A, Henein H. Mold Slag Property Measurements to Characterize Continuous-Casting Mold – Shell Gap Phenomena. *Canadian Metallurgical Quarterly* 2006; 45(1): 79-94.
22. *ABAQUS User Manuals v6.7.* Simulia Inc. 2007.
23. Park JK, Thomas BG, Samasekera IV. Analysis of thermomechanical behavior in billet casting with different mould corner radii. *Ironmaking and Steelmaking* 2002;29.
24. Han, HN, Lee JE, Yeo TJ, Won YM, Kim K, Oh KH and Yoon JK. A Finite element model for 2-dimensional slice of cast strand. *ISIJ International* 1999; 39(5):445-455.
25. L.C. Hibbeler, B.G. Thomas, B. Santillana, A. Hamoen, A. Kamperman, Longitudinal Face Crack Prediction with Thermo-Mechanical Models of Thin-Slabs in Funnel Moulds, La Metallurgia Italiana, in press, Feb., 2009
26. Hibbeler L.C., Koric S., Xu K., Thomas B.G., Spangler C., Thermo-Mechanical Modeling of Beam Blank Casting, AISTech Iron and Steel Technology Conference 2008, Pittsburgh, PA